

Supplementary Figures

Comparative phosphoproteomic analysis reveals the response of starch metabolism to high-temperature stress in rice endosperm

Yuehan Pang¹, Yaqi Hu¹ and Jinsong Bao^{1*}

1 Institute of Nuclear Agricultural Sciences, College of Agriculture and Biotechnology, Zhejiang University, Zijingang Campus, Hangzhou, 310058, China

* Correspondence: jsbao@zju.edu.cn

Figure S1. Temperature variation of control and high-temperature treatment groups in artificial climatic chambers.

Figure S2. (a) Experimental design for the phosphoproteome of rice endosperm in response to heat stress. (b) Mass error distribution of all identified peptides. (c) Peptide length distribution. (d) Heatmap of the Pearson correlation among the samples from different biological replicates.

Figure S3. Upset plots and Venn diagrams of significantly differentially phosphosites (a) and phosphoproteins (b) in 9311-C, 9311-H, GLA4-C, and GLA4-H.

Figure S4. (a) The percentage of kinases detected in our study and the rice protein database. Significantly enriched kinase families in phosphoproteome were labeled with an asterisk ($P<0.05$). (b) Summary of kinases with significant differences in response to heat stress. Venn diagram at left compares the identified kinases between the two varieties, whereas the right depicting the overlap of significantly differentially phosphosites in 9311-C, 9311-H, GLA4-C, and GLA4-H.

Figure S5. Enrichment analysis based on gene ontology (GO) terms and KEGG pathway. (a-b) GO biological process (GO-BP) and GO molecular function (GO-MF) enrichment analysis. Enrichment networks from four significantly deregulated groups were visualized using Cytoscape plugins Enrichment Map with different colors. Each node represents an enriched GO term, and the node size corresponds to the number of phosphoproteins. Edge thickness shows the overlap of GO terms between neighbor nodes. (c) KEGG enrichment analysis of differentially phosphorylated proteins of 9311 and GLA4.

Figure S6. Transcription factors identified in phosphoproteome.

Figure S7. Western blot assay of GBSSI at the three grain-filling stages. Western blots were performed three independent times, and the best blot was shown. The results of the independent experiments were following a similar trend in expression. Uncropped western

blots are available in Figure S20.

Figure S8. Evaluation of the protein level expression of starch synthesis related enzymes at the three grain-filling stages. The relative expression was normalized using plant actin. *P<0.05, **P<0.01, ***p<0.001, ****p<0.0001

Figure S9. Domain structure of SSIIa and SSIIIa and their phosphosites with significant differences in response to heat stress.

Figure S10. Domain structure and amino acid sequence alignments of PHO1. Residues in yellow indicate the phosphorylation site. Non-phosphorylated residues are shown in dark grey.

Figure S11. (a) Regulatory relationships between phosphorylated regulatory factors and their target genes in rice endosperm. Blue and red arrows indicate activation and suppression, respectively. The black dotted line represents homologous regulators of other cereal crops. (b) Potential target phosphosites of SPK in sucrose synthase. Residues in orange indicate the phosphorylation site. Non-phosphorylated residues are shown in dark grey.

Figure S12. Mass spectrometry of synthetic phosphorylated peptides.

Figure S13. Blocking peptide experiments show the specificity of the phosphor antibodies. Immunolabeling was virtually eliminated by phosphorylated peptide blocking. PBP, phosphorylated peptide blocking; NBP, non-phosphorylated peptide blocking.

Figure S14. Phosphorylation levels of SSIIIa-S94, BEI-S562, BEI-S620, BEI-S821, BEIIb-S685, and BEIIb-S715 detected by LC-MS/MS and western blot at 10 DAF. The intensity of LC-MS/MS was obtained from Table S2. The relative expression by western blot was normalized using plant actin, and the phosphorylation levels presented here were not corrected by corresponding total protein for a more intuitive comparison with LC-MS/MS results.

Figure S15. The number of phosphosites (phosphoproteins) detected in each kinase subfamily.

Figure S16. Spliceosome pathway by KEGG. The orange shading represents phosphoproteins identified.

Figure S17. Domain structure and amino acid sequence alignments of RSZp21a, RSZp21b, and RSZp23. Residues in orange indicate the phosphorylation site. Non-phosphorylated residues are shown in dark grey.

Figure S18. Heatmap of normalized phosphorylation intensity and relative expression foldchange of SR proteins (RSZp21a, RSZp21b, and RSZp23) under high-temperature stress.

Figure S19. Uncropped western blots of Figure 7. Red boxes in the uncropped blots indicate the cropped regions shown in the corresponding Figures.

Figure S20. Uncropped western blots of Figure S7. Red boxes in the uncropped blots indicate the cropped regions shown in the corresponding Figures.

Figure S1

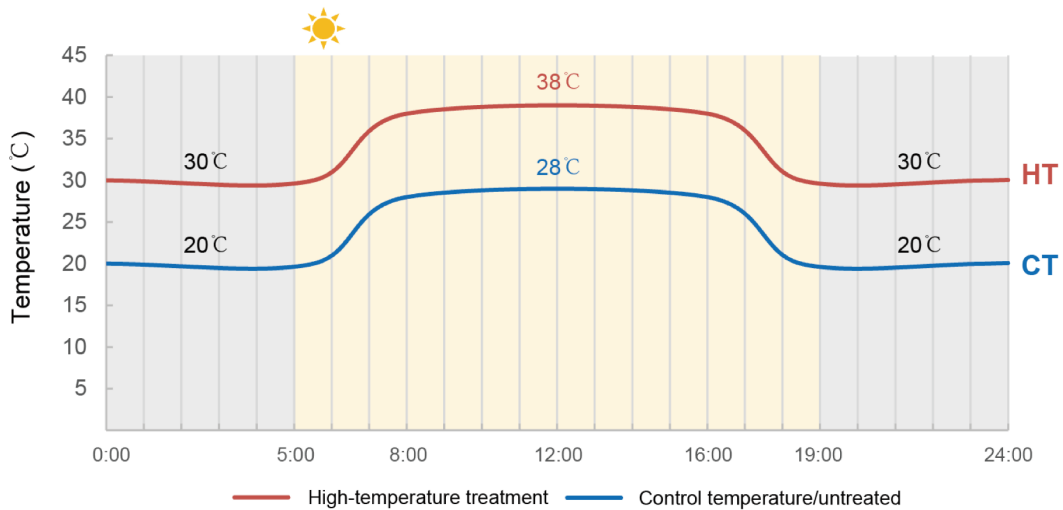
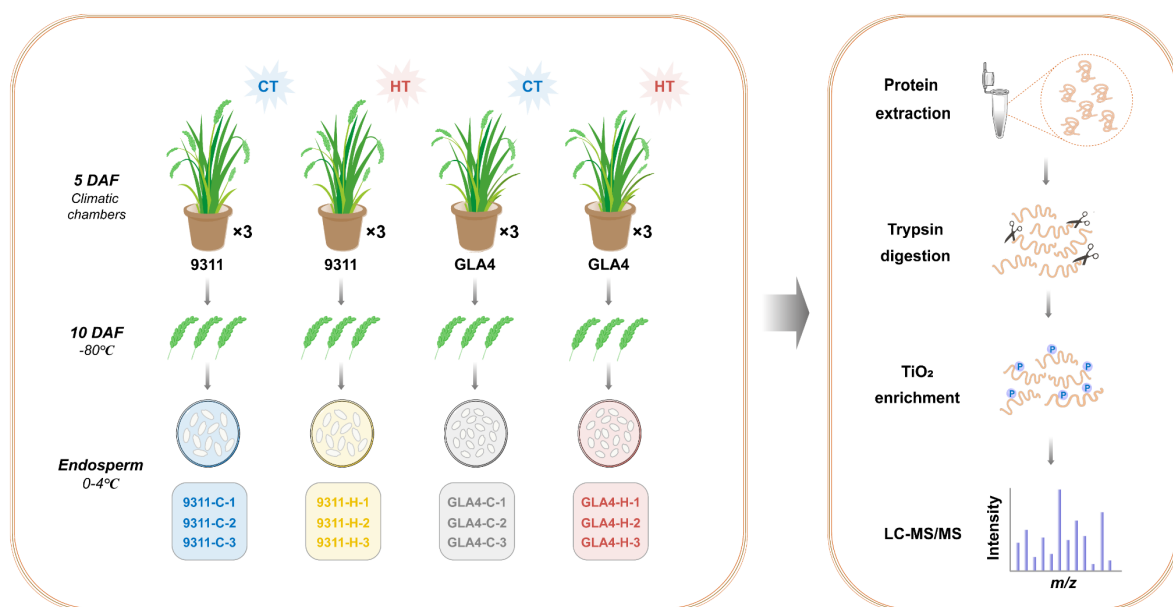
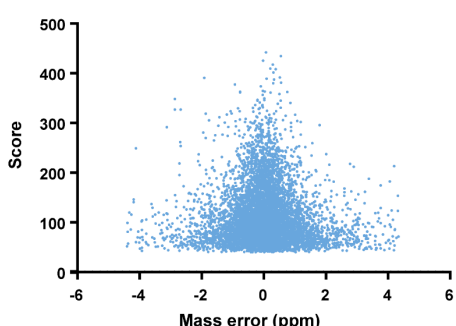


Figure S2

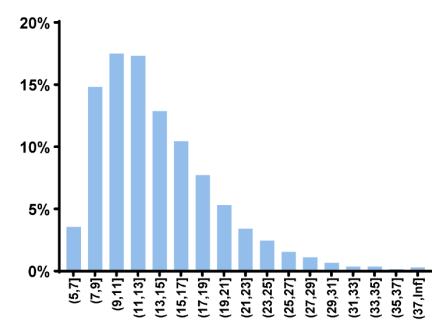
(a)



(b)



(c)



(d)

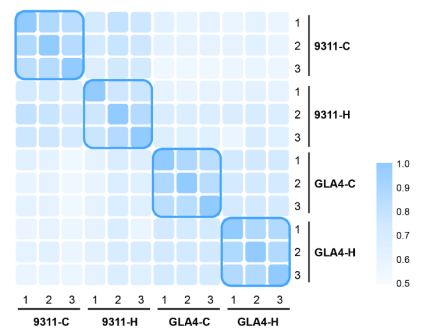
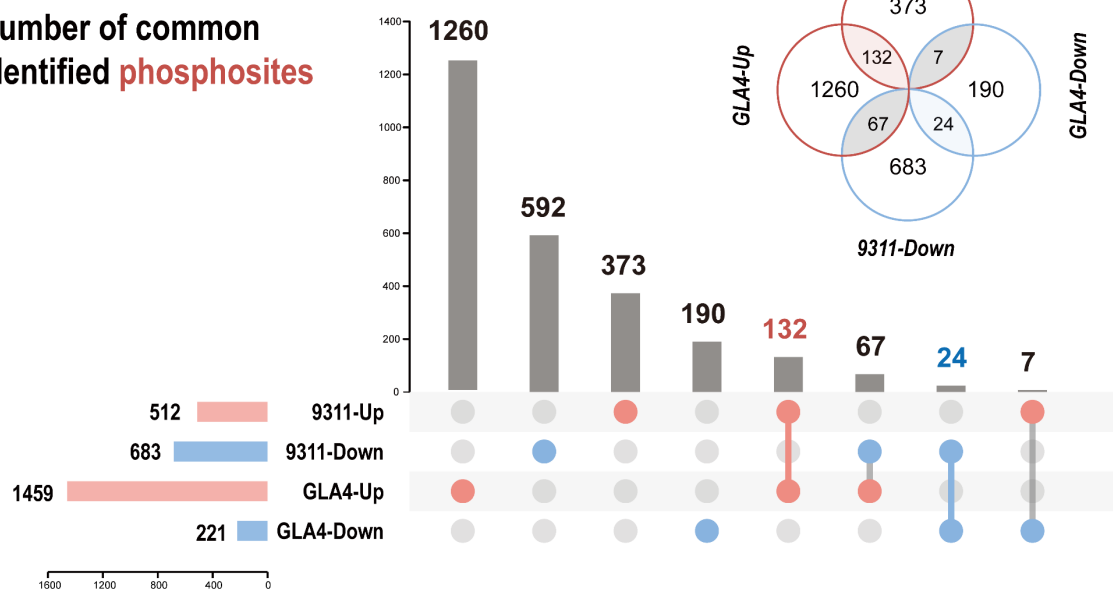


Figure S3

(a)

Number of common identified phosphosites



(b)

Number of common identified phosphoproteins

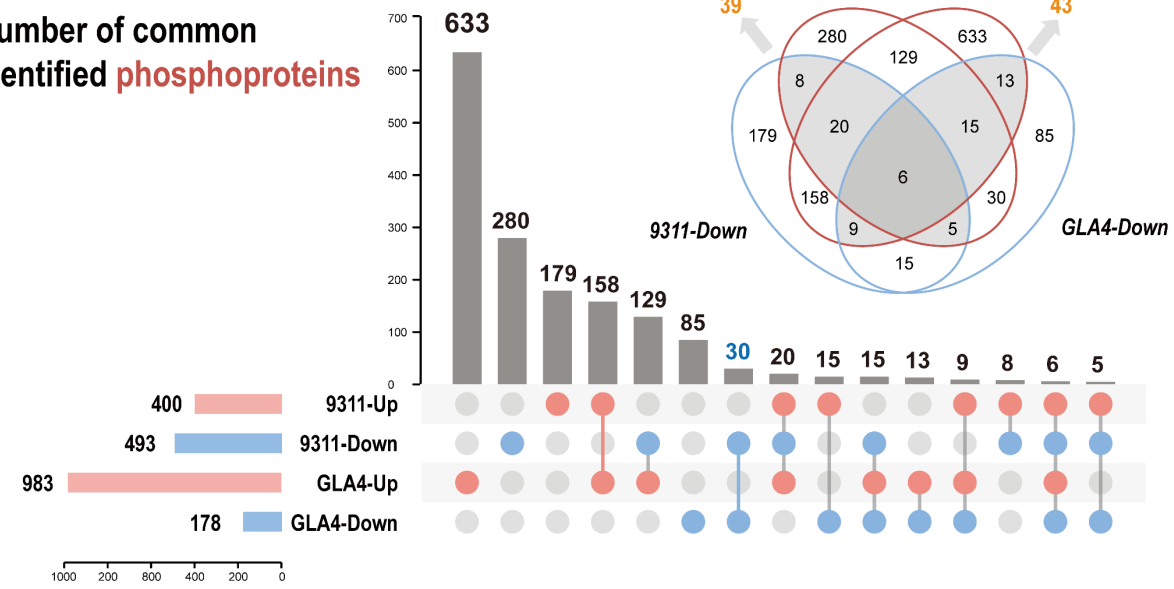


Figure S4

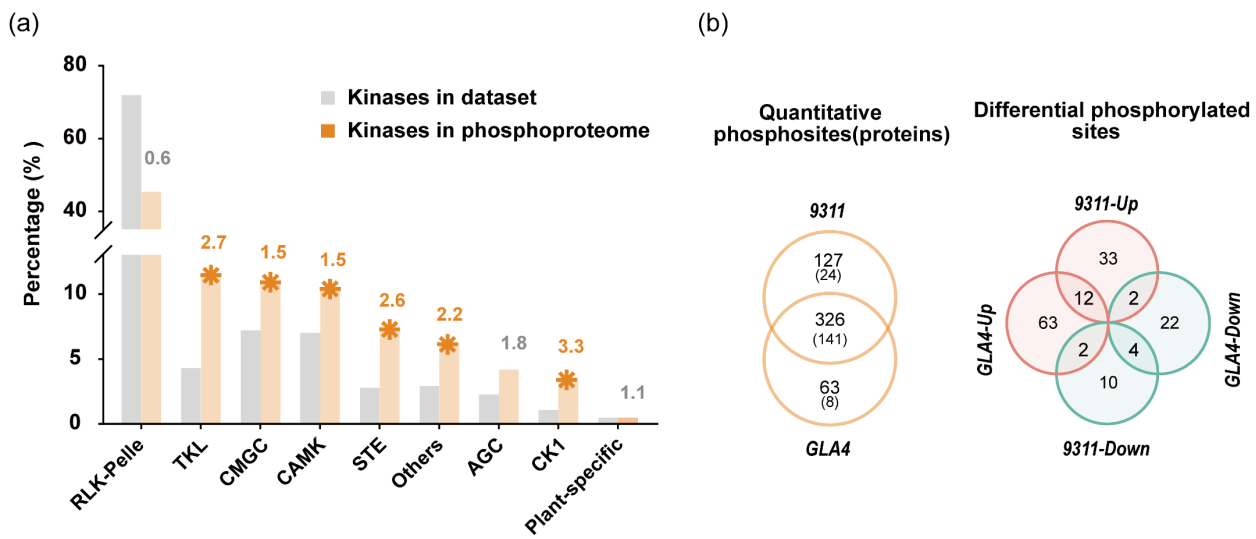


Figure S5

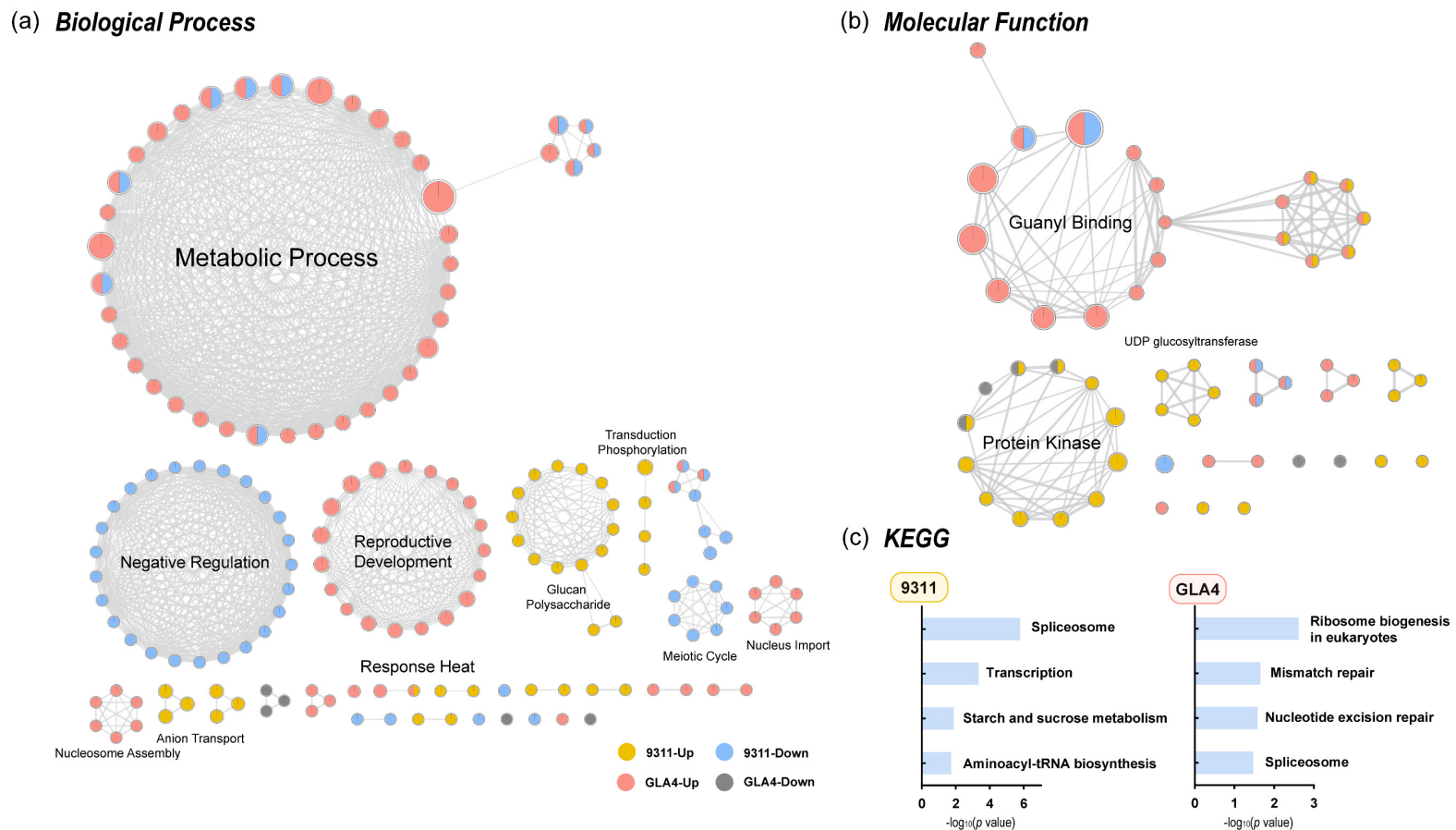


Figure S6

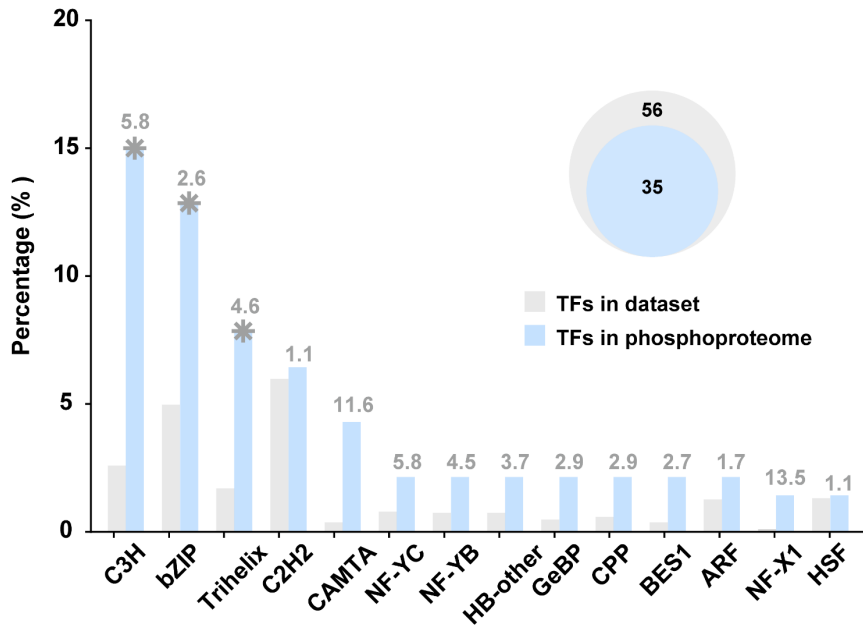


Figure S7

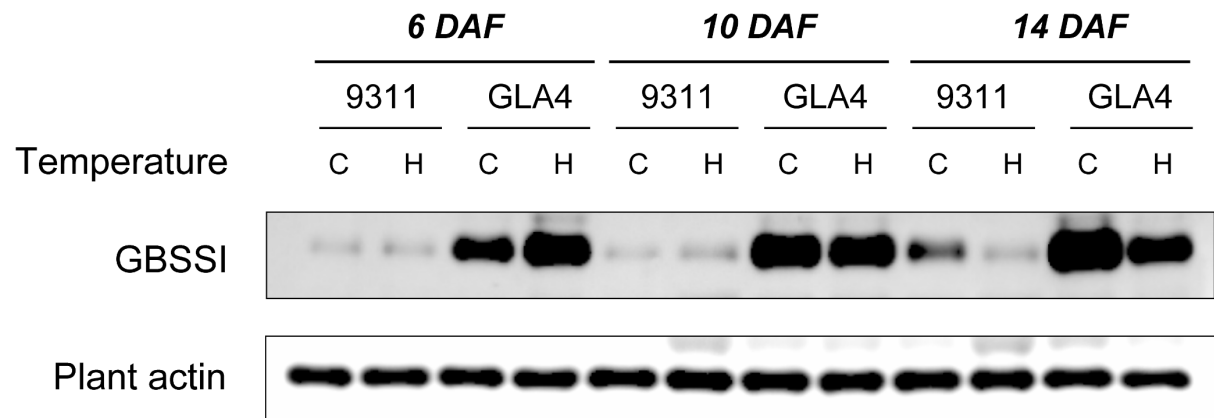


Figure S8

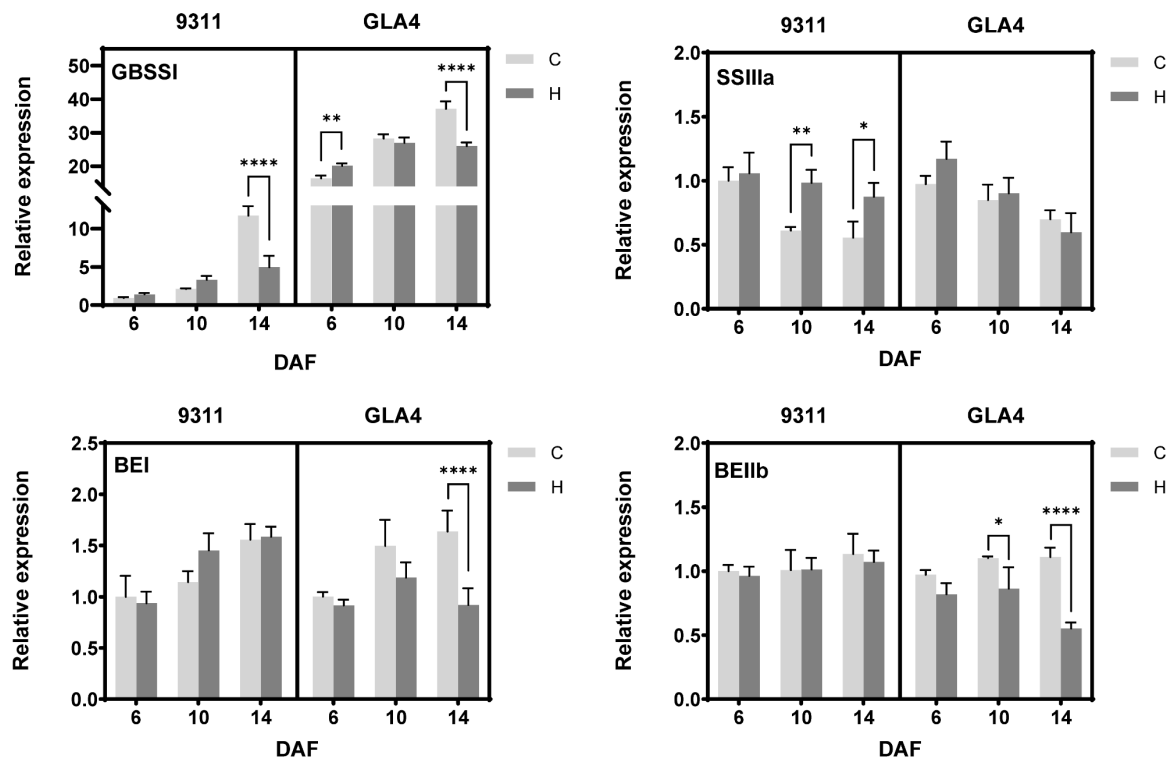


Figure S9

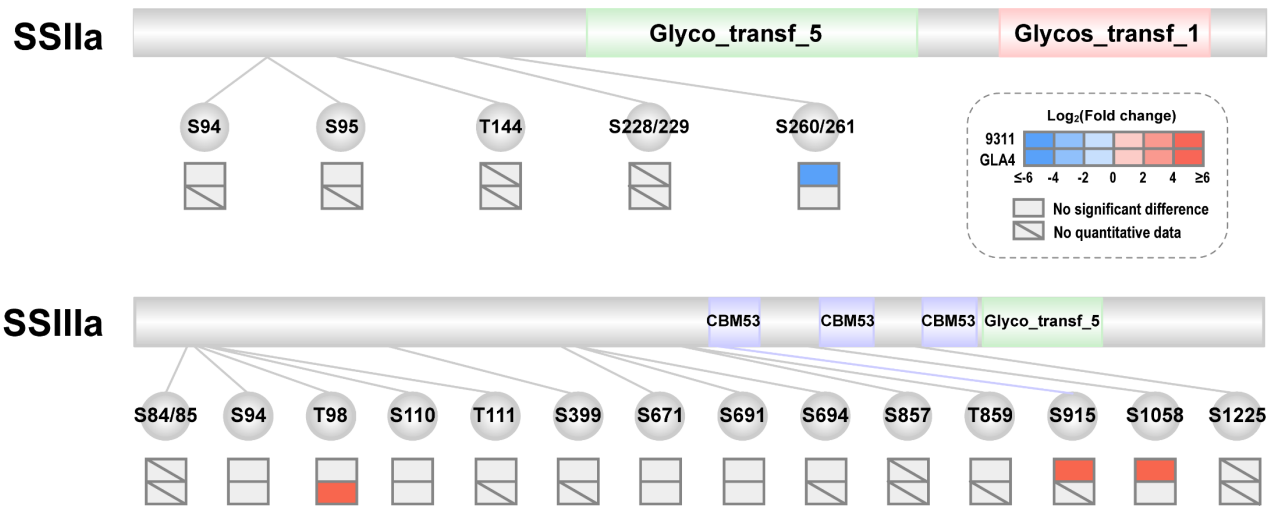


Figure S10

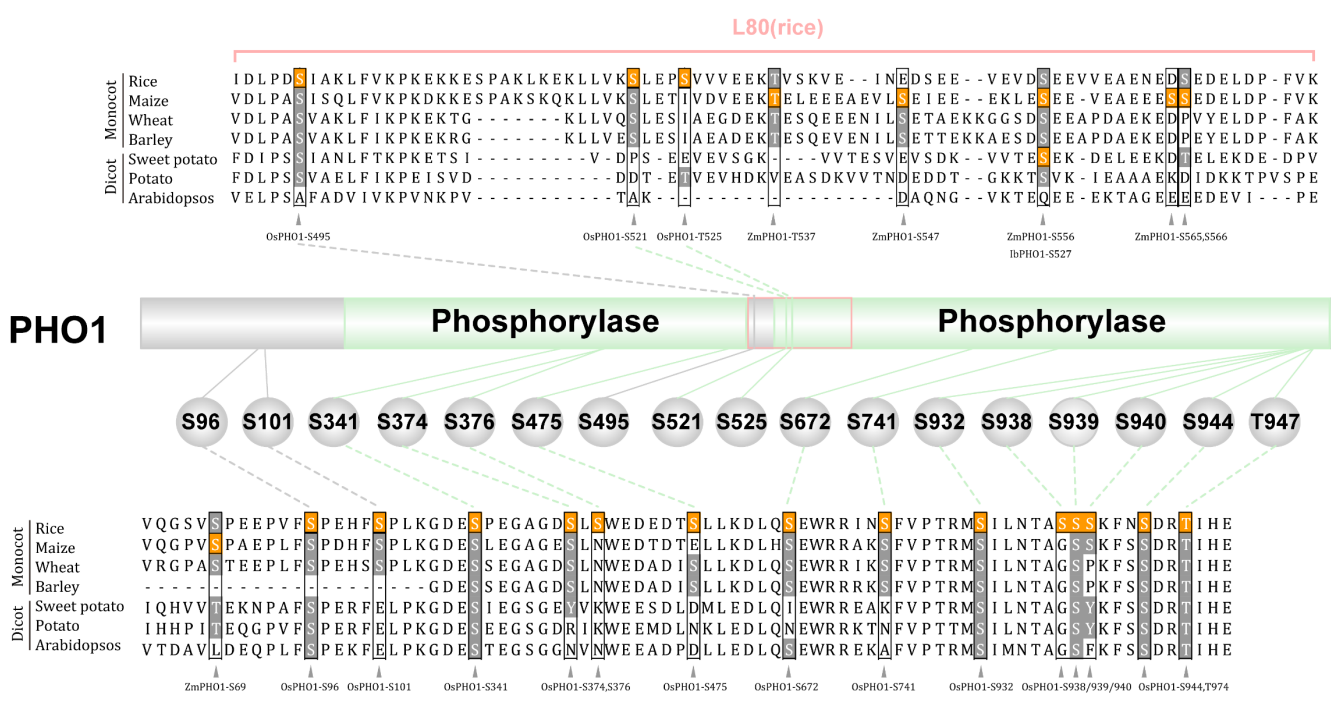
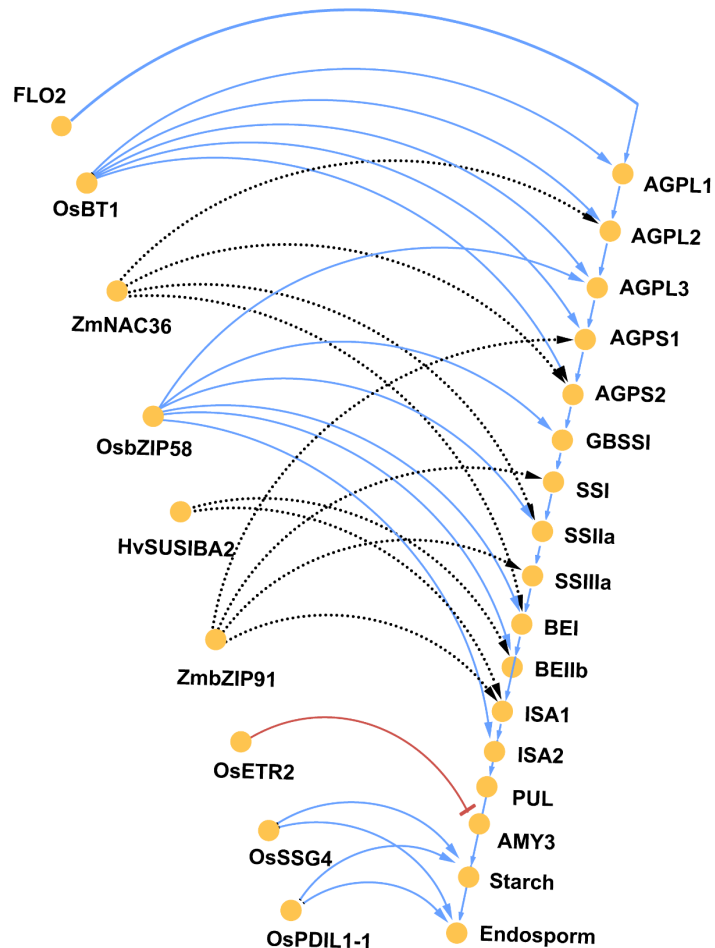


Figure S11

(a)



(b)

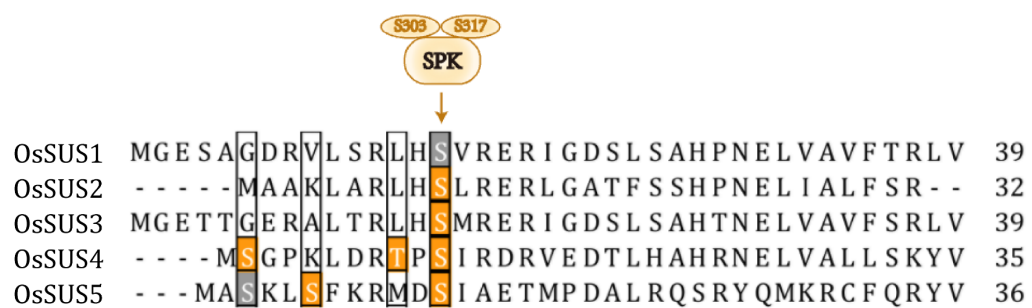


Figure S12

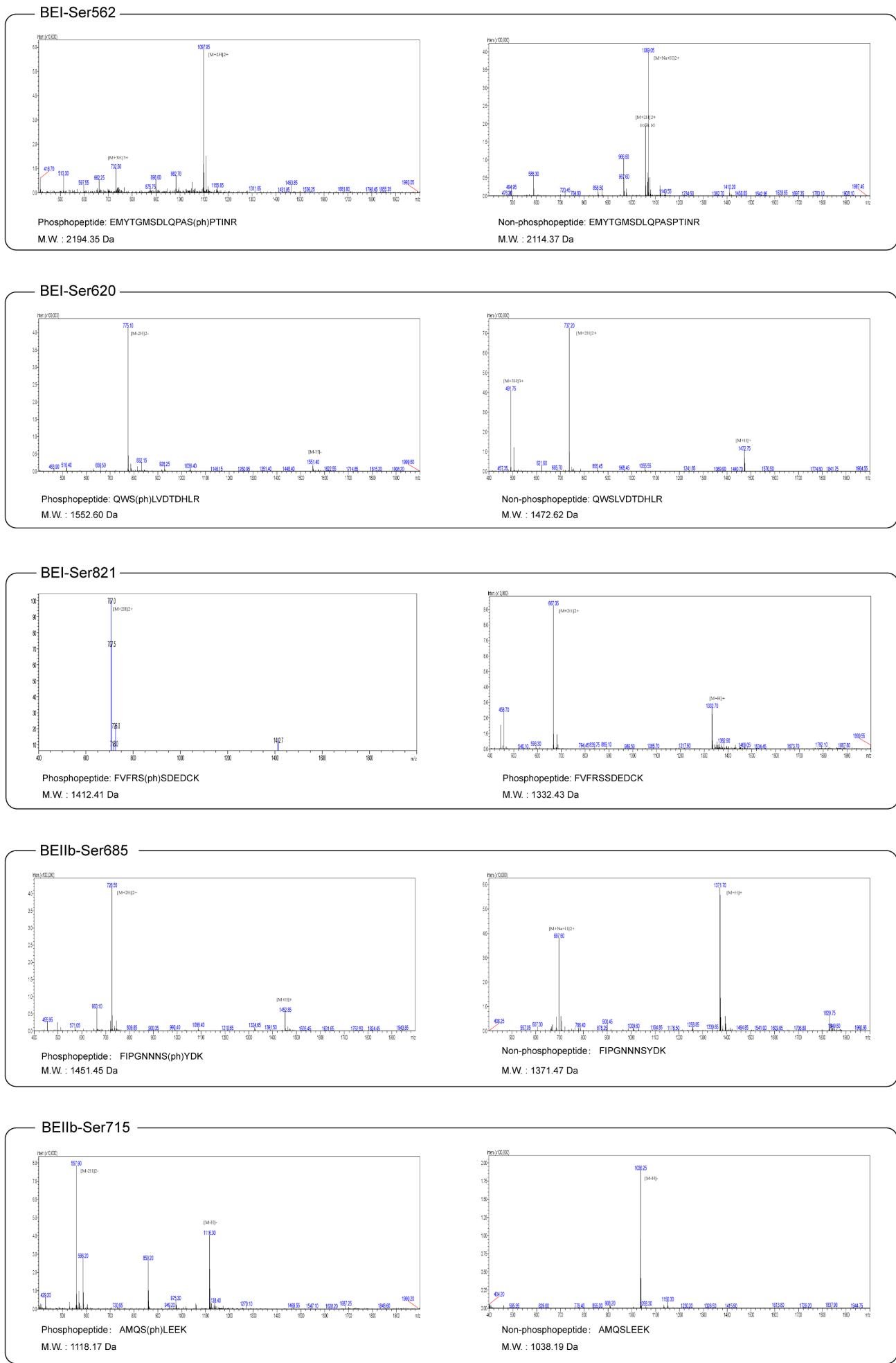


Figure S13

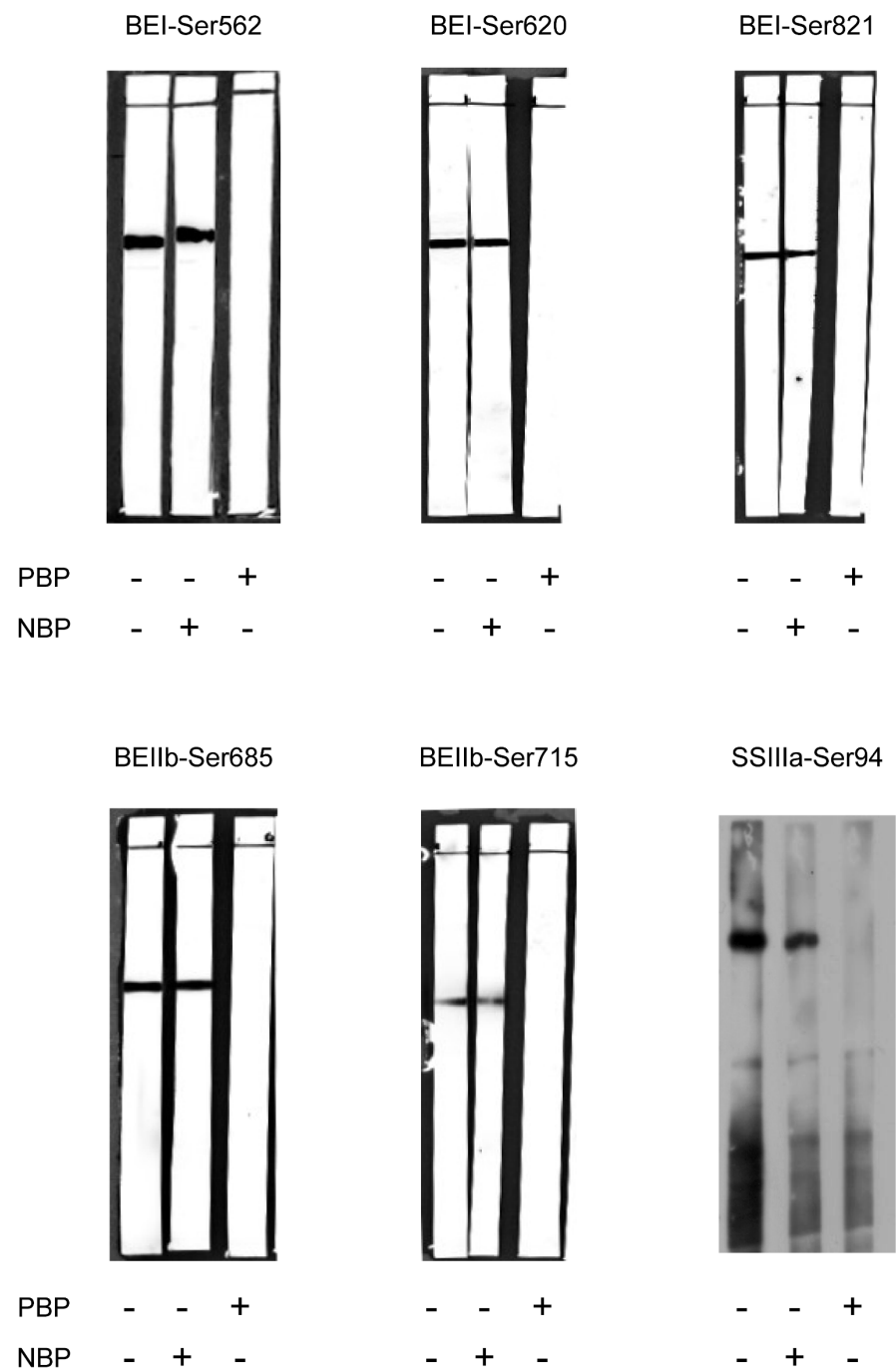


Figure S14

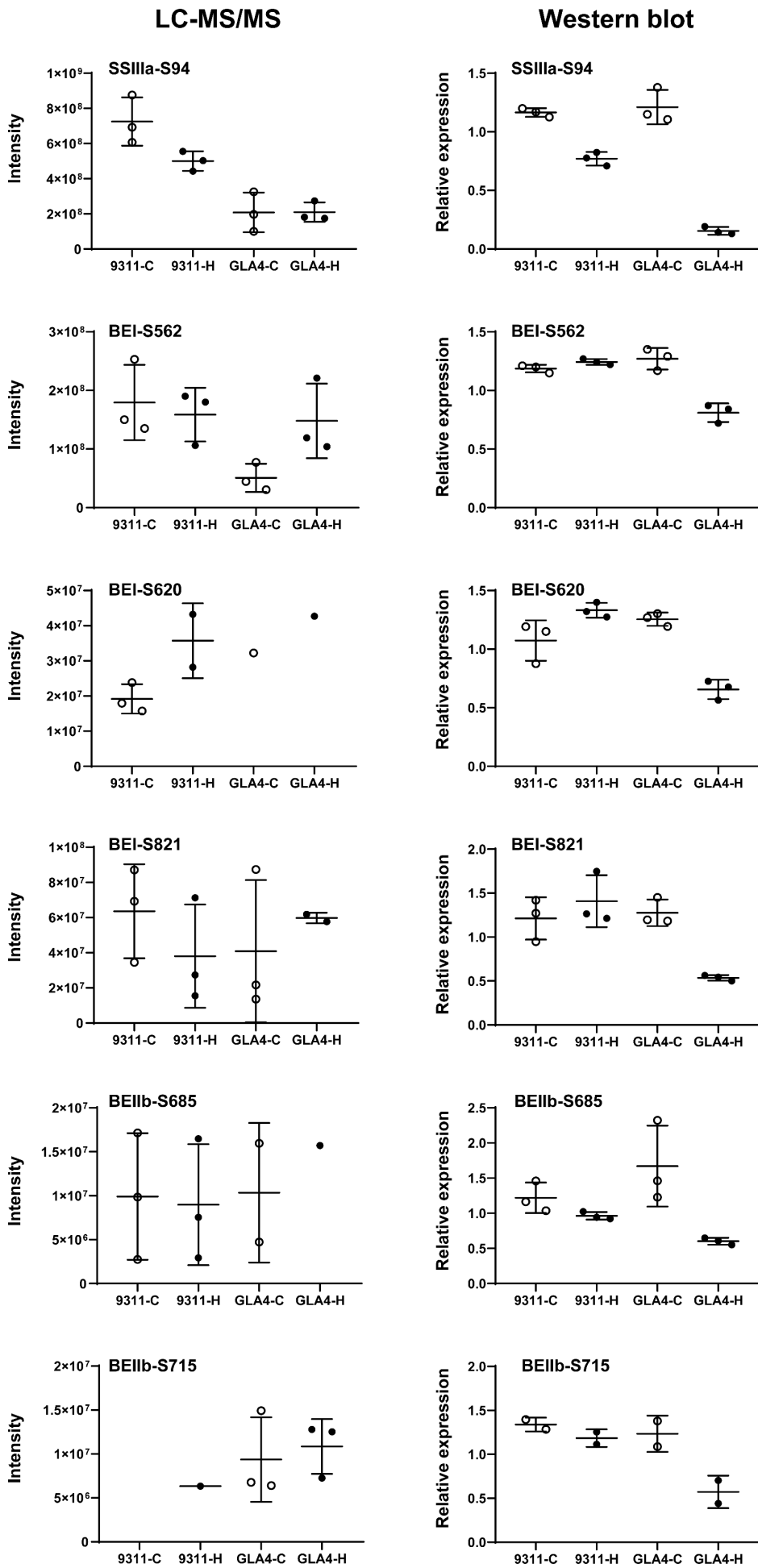


Figure S15

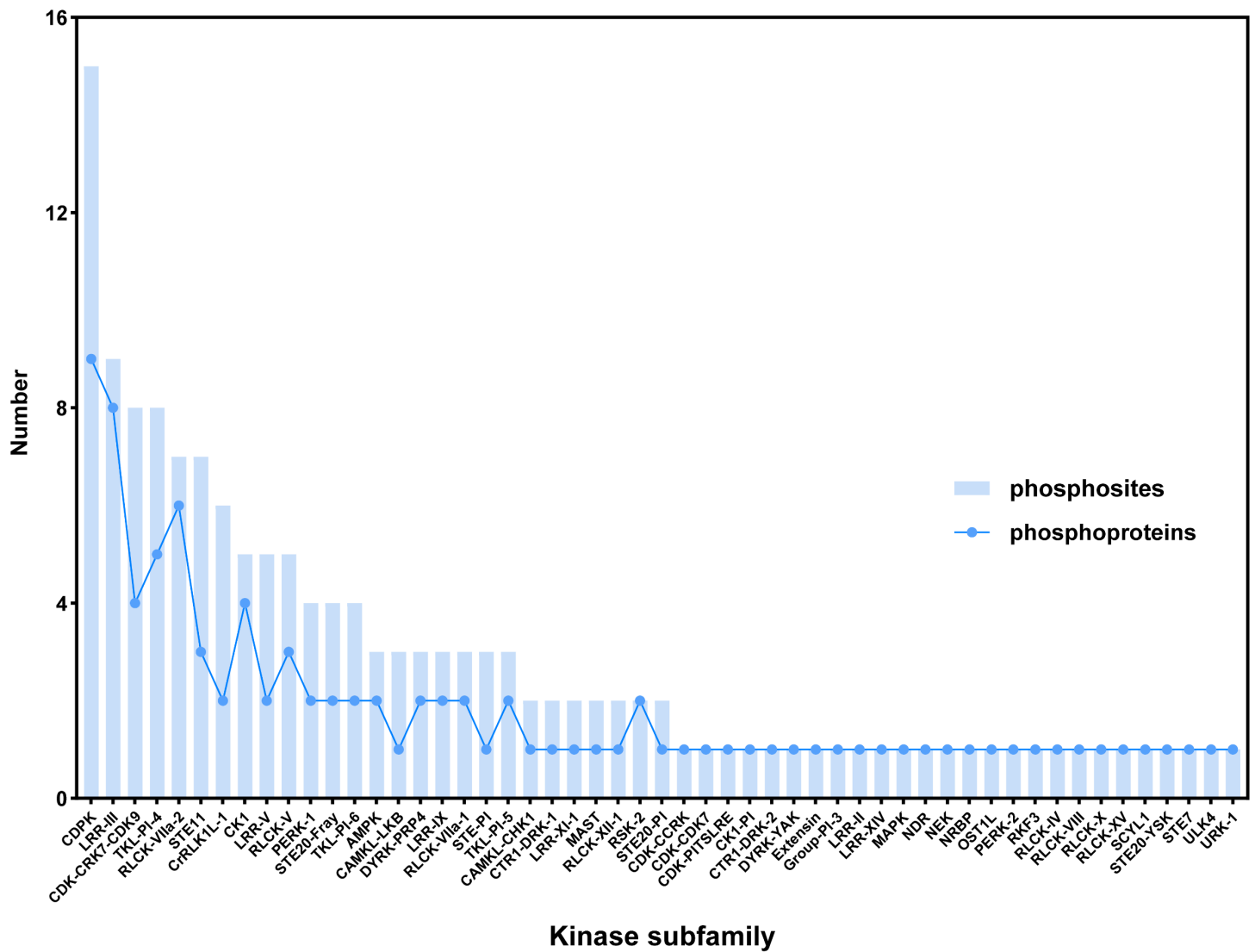


Figure S16

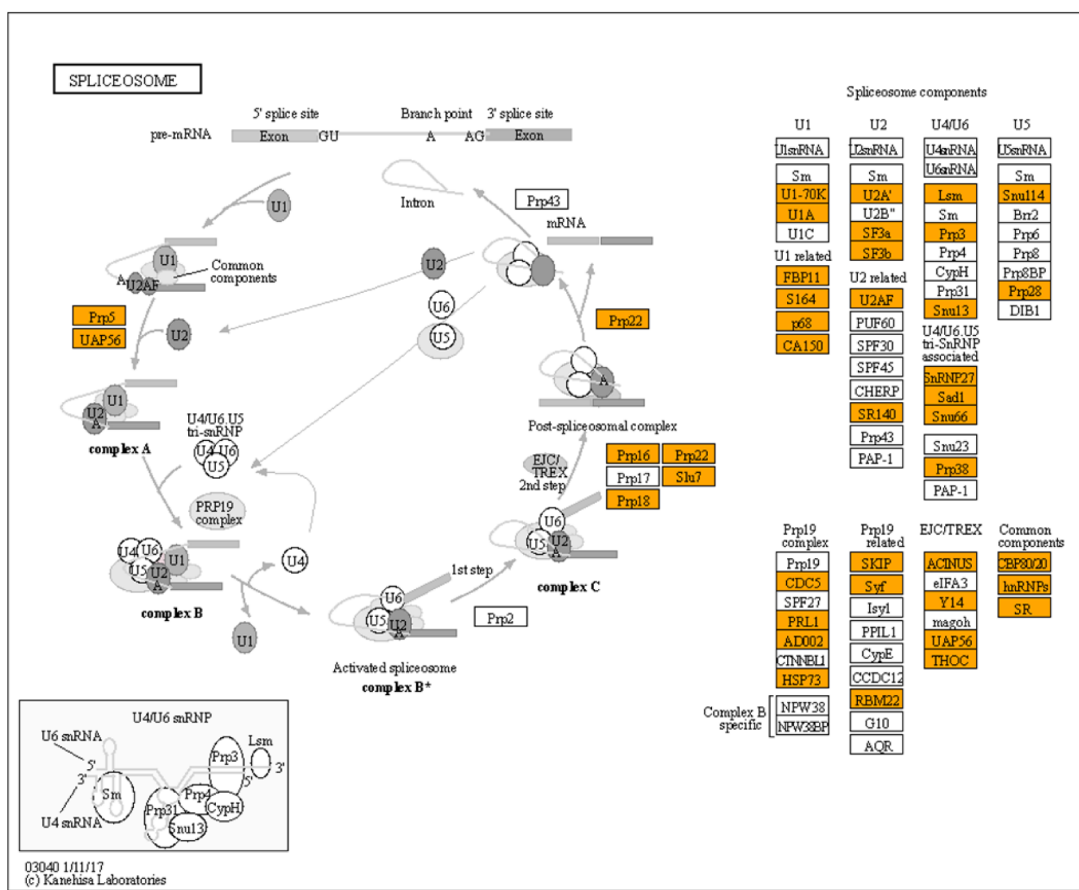


Figure S17

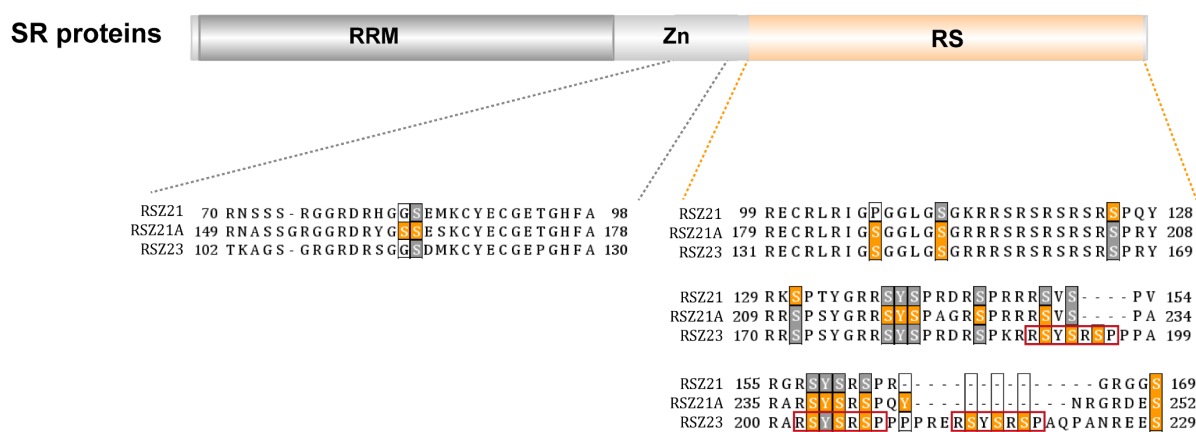


Figure S18

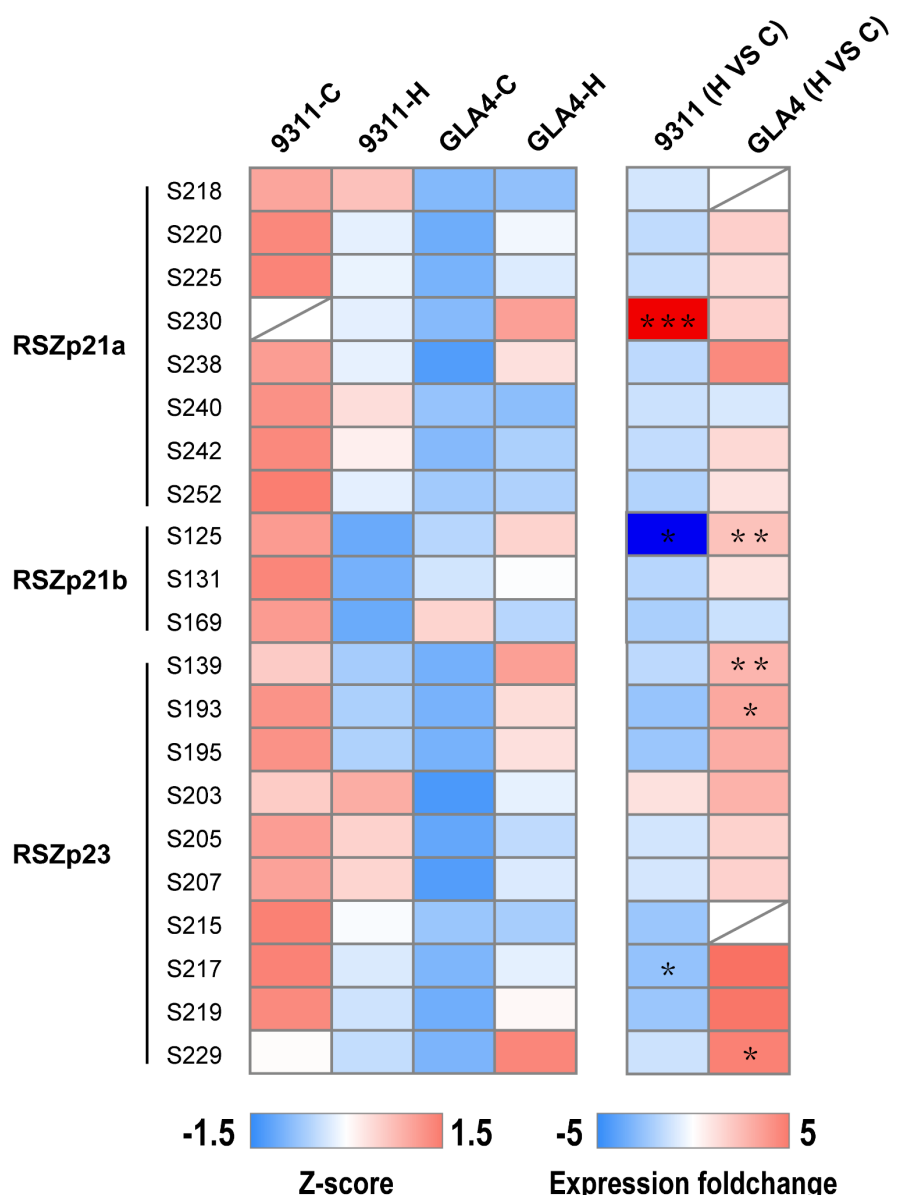


Figure S19

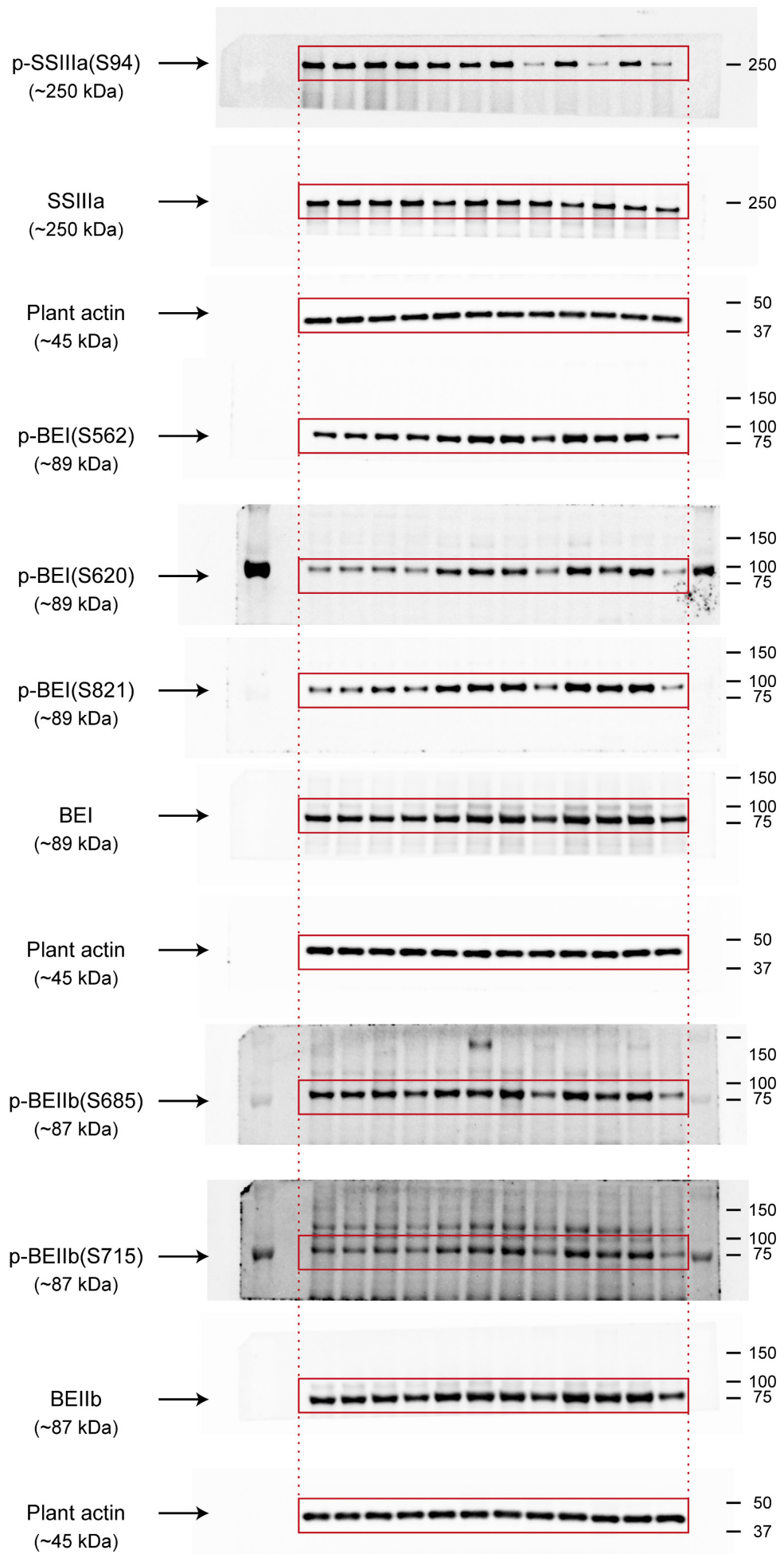


Figure S20

